Computation of Airfoils at Very Low Reynolds Numbers

Denis Bichsel*,[1] and Peter Wittwer[2]
[1]HESSO, Ecole d'Ingénieurs de Genève, [2]DPT, Université de Genève
*Corresponding author: 4, Rue de Prairie, 1202 Genève, Switzerland, denis.bichsel@hesge.ch

Abstract: We discuss a new numerical scheme involving adaptive boundary conditions which allows to compute, at very low Reynolds numbers, drag and lift of airfoils with rough surfaces efficiently with great precision. As an example we present the numerical implementation for an airfoil consisting of a line segment. The solution of the Navier-Stokes equations is singular at the leading and the trailing edge of this airfoil, and the computation of drag and lift by integration of the stress tensor along the segment therefore delicate. However, since for numerical purposes the infinite exterior domain has to be truncated to a finite computational domain anyway, this problem can be avoided by integrating not over the airfoil, but over the surface of the truncated domain instead. Together with the adaptive boundary conditions this allows to determine drag and lift with great precision already on small computational domains.

Keywords: Airfoils, low Reynolds numbers, drag, lift, artificial boundary conditions.

1. Introduction

The wish to construct aircraft that can fly at low Reynolds numbers is not new. Important publications which are concerned with the design of low speed airfoils and which are still of relevance today are [17], [5], [6], [11], [7], and [10]. When these papers were written, Reynolds numbers of the order of fifty to hundred thousand were considered small, but nowadays the interest focuses on flows with Reynolds number in the range from as low as some hundred to several thousand. Quite recently even a new experimental facility has been built with the specific goal of measuring flows for this range of Reynolds numbers. See [8]. The goal of these experimental works and of the corresponding theoretical studies is the engineering of so-called micro-air vehicles (MAV). There is an extensive recent literature on the subject. See in particular [15], [1], [13], and [14]. An important ingredient for the design of MAV's is the development of new types of airfoils, since at the very low Reynolds numbers under consideration the traditional NACA type profiles perform poorly. Wings made from flat plates and other designs with sharp corners produce much better results. One is therefore interested in computing drag and lift for this type of airfoils, but this turns out to be delicate for several reasons. First, neither linearized theories (Stokes, Oseen) nor any version of boundary layer theory [16], [5], [6] provide a quantitative description at the Reynolds numbers under consideration, so that the full Navier-Stokes equations need to be solved. Second, solutions are singular at non-smooth boundaries which makes the evaluation of the stress tensor for the determination of drag and lift problematic. Third, drag and lift of low Reynolds number flows are very sensitive to changes in boundary conditions. This is a serious problem, since for computational reasons the exterior domain needs to be truncated to a finite sub-domain, and this therefore leads to the necessity of finding boundary conditions on the surface of the truncated domain which do not modify drag and lift significantly.

In what follows we address these questions for the simple case of an airfoil which consists of a line segment. See Figure 1. We present here only the flow parallel to the segment which produces no lift, but the method is not limited to this case. More details can be found in [3], [4], and [9]. The basic ideas are the following. First, in order to avoid to have to integrate over the non-smooth boundary of the airfoil when computing drag and lift, one rather integrates over the outer boundary of the computational domain which we choose either to be a rectangle or a circle. Second, the boundary conditions on this outer boundary are chosen to be adaptive according to the

scheme introduced in [3].

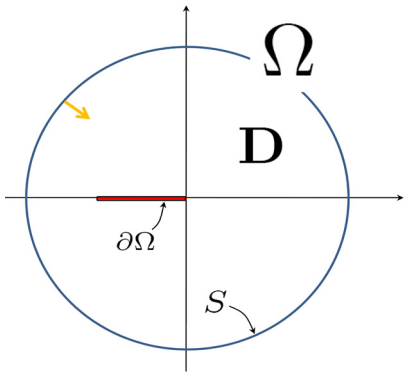

Fig. 1. The line segment (red), the exterior domain Ω, the computational domain $\mathbf{D}$, the boundary $\partial\Omega$, the exterior boundary S of the computational domain, and the orientation of the normal vector on S (yellow).

So, consider a line segment of length A that is placed into a uniform stream of a homogeneous incompressible fluid filling up all of $\mathbf{R}^2$. This situation is modeled by the stationary Navier-Stokes equations

$$-\rho\,(\mathbf{u}\cdot\boldsymbol{\nabla})\,\mathbf{u}+\mu\Delta\mathbf{u}-\boldsymbol{\nabla}p=0\ , \qquad (1)$$

$$\boldsymbol{\nabla}\cdot\mathbf{u}=0\ , \qquad (2)$$

in $\Omega=\mathbf{R}^2\setminus[0,A]$, subject to the boundary conditions

$$\mathbf{u}|_{\partial\boldsymbol{\Omega}}=0\ , \qquad (3)$$

$$\lim_{|\mathbf{x}|\to\infty}\mathbf{u}(\mathbf{x})=\mathbf{u}_\infty\ . \qquad (4)$$

Here, $\mathbf{u}$ is the velocity field, p is the pressure and $\mathbf{u}_\infty$ is some constant non-zero vector field which we choose without restriction of generality to be parallel to the x-axis, *i.e.*, $\mathbf{u}_\infty=u_\infty\mathbf{e}_1$, where $\mathbf{e}_1=(1,0)$ and $u_\infty>0$. The density ρ and the viscosity μ are positive constants. From μ, ρ and u_∞ we can form the length ℓ,

$$\ell=\frac{\mu}{\rho u_\infty}\ , \qquad (5)$$

the so called viscous length of the problem. For the Reynolds based on chord length we therefore have

$$\mathrm{Re}=\frac{A}{\ell}\ . \qquad (6)$$

2. Theoretical aspects

The flow around a line segment has been intensively studied in the literature. See [12] for a review. Boundary layer theory based on the Blasius solution of a semi-infinite plate predicts (see [2] for a review) that the drag coefficient $C_{\mathrm{Drag}}=F/(\frac{1}{2}\rho A u_\infty^2)$, with F the total drag of the finite plate, should be given, asymptotically for large values of Re, by the formula

$$\tfrac{1}{2}C_{\mathrm{Drag}}\approx 1.328\,\mathrm{Re}^{-1/2}+C_1\ \mathrm{Re}^{-1}\ , \qquad (7)$$

with a value for the constant C_1 which was estimated at 2.6 ± 0.1 in early work and then at 4.5 ± 0.5. The more sophisticated so called triple deck solution for the finite plate, which was developed later with the goal of explaining the discrepancies between the prediction (7) and experimental and numerical data, takes the contribution from the trailing edge singularity into account. This leads to the new prediction that

$$\tfrac{1}{2}C_{\mathrm{Drag}}\approx 1.328\,\mathrm{Re}^{-1/2}+(2.661\pm0.03)\,\mathrm{Re}^{-7/8} \qquad (8)$$

See [12]. Expression (8) is a priori again an asymptotic description valid at large Reynolds numbers only, but turns out to be surprisingly accurate all the way down to Reynolds numbers of order one. See below for details.

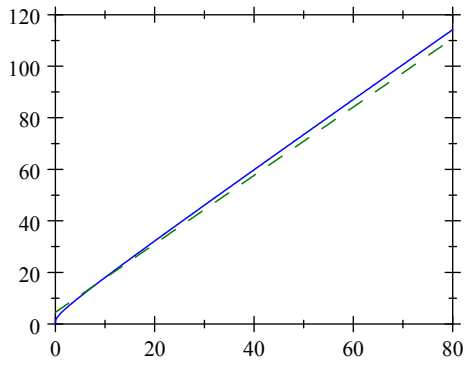

Fig. 2. Theoretical prediction of $\frac{1}{2}C_{\mathrm{Drag}}\,\mathrm{Re}$ as a function of $\mathrm{Re}^{1/2}$. The dashed green curve is the theory given by (7) and the blue curve the prediction of the triple deck theory (8).

3. Computation of drag and lift

We briefly recall the computation of drag and lift through surface integrals. Let $\mathbf{u}$, p be a solution of the Navier-Stokes equations (1), (2) subject to the boundary conditions (3), (4), and let $\mathbf{e}$ be some arbitrary unit vector

in $\mathbf{R}^2$. Multiplying (1) with $\mathbf{e}$ leads to

$$-(\mathbf{u}\cdot\boldsymbol{\nabla})(\mathbf{u}\cdot\mathbf{e})+\Delta(\mathbf{u}\cdot\mathbf{e})-\boldsymbol{\nabla}\cdot(p\mathbf{e})=0\ . \tag{9}$$

Since

$$\begin{aligned}&\boldsymbol{\nabla}\cdot((\mathbf{u}\cdot\mathbf{e})\,\mathbf{u})\\&=\mathbf{u}\cdot(\boldsymbol{\nabla}(\mathbf{u}\cdot\mathbf{e}))+(\mathbf{u}\cdot\mathbf{e})(\boldsymbol{\nabla}\cdot\mathbf{u})\\&=(\mathbf{u}\cdot\boldsymbol{\nabla})(\mathbf{u}\cdot\mathbf{e})\ ,\end{aligned}$$

and

$$\Delta(\mathbf{u}\cdot\mathbf{e})=\boldsymbol{\nabla}\cdot(\ [\boldsymbol{\nabla}\mathbf{u}+(\boldsymbol{\nabla}\mathbf{u})^T]\cdot\mathbf{e})\ ,$$

equation (9) can be written as $\boldsymbol{\nabla}\cdot\mathbf{P}(\mathbf{e})=0$, where

$$\mathbf{P}(\mathbf{e})=-(\mathbf{u}\cdot\mathbf{e})\,\mathbf{u}+[\boldsymbol{\nabla}\mathbf{u}+(\boldsymbol{\nabla}\mathbf{u})^T]\cdot\mathbf{e}-p\mathbf{e}\ , \tag{10}$$

i.e., the vector field $\mathbf{P}(\mathbf{e})$ is divergence free. Therefore, applying Gauss' theorem to the region $\mathbf{D}$ in Figure 1 we find that

$$\int_{\partial\Omega}\mathbf{P}(\mathbf{e})\cdot\mathbf{n}\ d\sigma=-\int_S\mathbf{P}(\mathbf{e})\cdot\mathbf{n}\ d\sigma\ , \tag{11}$$

with the choice of the normal vector on S as indicated in Figure 1. We have that $\mathbf{P}(\boldsymbol{\varepsilon}_1)\cdot\boldsymbol{\varepsilon}_2=\mathbf{P}(\boldsymbol{\varepsilon}_2)\cdot\boldsymbol{\varepsilon}_1$ for any two unit vectors $\boldsymbol{\varepsilon}_1$ and $\boldsymbol{\varepsilon}_2$, and therefore, since in (11) the vector $\mathbf{e}$ is arbitrary, it follows that

$$\int_{\partial\Omega}\mathbf{P}(\mathbf{n})\ d\sigma=-\int_S\mathbf{P}(\mathbf{n})\ d\sigma\ . \tag{12}$$

Since $\mathbf{u}=0$ on $\partial\Omega$, we finally get from (10) and (12) that the total force on the airfoil is either given by an integral of the stress tensor $\Sigma(\mathbf{u},p)=\mu\left[\boldsymbol{\nabla}\mathbf{u}+(\boldsymbol{\nabla}\mathbf{u})^T\right]-p$ over the surface $\partial\Omega$ of the airfoil,

$$\mathbf{F}=\int_{\partial\Omega}\Sigma(\mathbf{u},p)\cdot\mathbf{n}\ d\sigma\ , \tag{13}$$

or equivalently by an integral over the outer surface S of the computational domain $\mathbf{D}$,

$$\mathbf{F}=-\int_S(-\rho(\mathbf{u}\cdot\mathbf{n})\,\mathbf{u}+\Sigma(\mathbf{u},p)\cdot\mathbf{n})\ d\sigma\ . \tag{14}$$

The force $\mathbf{F}$ is traditionally decomposed into a component F parallel to the flow at infinity called drag and a component L perpendicular to the flow at infinity called lift. Note that $\mathbf{F}$ is independent of the choice of S.

4. Adaptive boundary conditions

When restricting for numerical purposes the equations from the exterior infinite domain Ω to a bounded domain $\mathbf{D}\subset\Omega$, one is confronted with the necessity of finding appropriate boundary conditions on the surface $S=\partial\mathbf{D}\setminus\partial\boldsymbol{\Omega}$ of the truncated domain. We set

$$\mathbf{u}|_S=\mathbf{u}_{ABC}|_S\ , \tag{15}$$

with $\mathbf{u}_{ABC}$ a vector field that is explicitly given below. The vector field $\mathbf{u}_{ABC}$ depends on drag and lift and these quantities are computed as part of the solution process. Note that for a finite computational domain $\mathbf{D}$ the boundary conditions on S fix the mass flux through the surface S. As has been shown in [18] there is a direct connection between drag, lift and this mass flux, and as a consequence any choice of boundary conditions which does not respect the correct mass flux changes the forces significantly, unless oversized computational domains are used. The adaptive boundary conditions (15) eliminate this problem. More details can be found below and in [3] and [4]. We set

$$\mathbf{u}_{ABC}(\mathbf{x})=u_\infty\ \mathbf{u}_N(\frac{\mathbf{x}}{\ell})\ , \tag{16}$$

with u_∞ the speed at infinity, with ℓ as given in (5), and with $\mathbf{u}_N$ the adaptive boundary conditions of order N,

$$\mathbf{u}_N(x,y)=(1,0)+\sum_{n=1}^{N}\sum_{m=1}^{n}\mathbf{u}_{n,m}(x,y)\ , \tag{17}$$

which we now define. Let $\mathbf{u}_{n,m}=(u_{n,m},v_{n,m})$. To first order we have

$$\begin{aligned}u_{1,1}(x,y)&=u_{1,1,E}(x,y)-\theta(x)\frac{d}{\sqrt{\pi}}\frac{1}{\sqrt{x}}e^{-\frac{y^2}{4x}}\ ,\\v_{1,1}(x,y)&=v_{1,1,E}(x,y)-\theta(x)\frac{d}{2\sqrt{\pi}}\frac{y}{x^{3/2}}e^{-\frac{y^2}{4x}}\end{aligned} \tag{18}$$

with θ the Heaviside function (i.e., $\theta(x)=1$ for $x>0$ and $\theta(x)=0$ for $x<0$), and

$$\begin{aligned}u_{1,1,E}(x,y)&=\frac{d}{\pi}\frac{x}{x^2+y^2}+\frac{b}{\pi}\frac{y}{x^2+y^2}\ ,\\v_{1,1,E}(x,y)&=\frac{d}{\pi}\frac{y}{x^2+y^2}-\frac{b}{\pi}\frac{x}{x^2+y^2}\ .\end{aligned} \tag{19}$$

The constants d and b are linked to drag and lift be the equations

$$d=\frac{1}{2}\frac{1}{\rho\ell u_\infty^2}F\ , \tag{20}$$

$$b=\frac{1}{2}\frac{1}{\rho\ell u_\infty^2}L\ , \tag{21}$$

and, as indicated above, the force $\mathbf{F} = (F, L)$ is computed as part of the solution process using (14) , which in turn allows us to update the boundary conditions on S using (20) and (21). Note that the vector field $(u_{1,1}, v_{1,1})$ in (18) is divergence free and smooth in $\mathbf{R}^2 \backslash \{0\}$. To second order we have

$$u_{2,1}(x,y) = \theta(x)\frac{bd}{2}\frac{1}{(\sqrt{\pi})^3}\frac{\log(x)}{x}\frac{y}{\sqrt{x}}e^{-\frac{y^2}{4x}} ,$$

$$v_{2,1}(x,y) = \theta(x)\frac{bd}{2}\frac{1}{(\sqrt{\pi})^3}\frac{1}{x^{3/2}}\cdot \left(\log(x)\left(-1+\frac{1}{2}\frac{y^2}{x}\right)+2\right)e^{-\frac{y^2}{4x}} , \quad (22)$$

and

$$u_{2,2}(x,y) = u_{2,2,E}(x,y) + \theta(x)d^2\frac{1}{x}f'(\frac{y}{\sqrt{x}}) + \lambda\theta(x)f_\infty d^2\frac{3}{8}\frac{1}{x^2}\cdot \left((1+\frac{|y|}{\sqrt{x}})(1-\frac{1}{2}\frac{y^2}{x})+\frac{|y|}{\sqrt{x}}\right)e^{-\frac{y^2}{4x}} ,$$

$$v_{2,2}(x,y) = v_{2,2,E}(x,y) + \theta(x)\frac{d^2}{2}\frac{1}{x^{3/2}}\cdot \left(f(\frac{y}{\sqrt{x}}) - f_\infty \mathrm{sign}(y) + \frac{y}{\sqrt{x}}f'(\frac{y}{\sqrt{x}})\right) + \lambda\theta(x)f_\infty d^2\frac{3}{4}\frac{1}{x^{5/2}}\cdot \left((1+\frac{|y|}{\sqrt{x}})\frac{y}{\sqrt{x}}(1-\frac{1}{8}\frac{y^2}{x}) + \frac{1}{4}\frac{y^2}{x}\mathrm{sign}(y)\right)e^{-\frac{y^2}{4x}} , \quad (23)$$

where

$$u_{2,2,E}(x,y) = f_\infty\frac{d^2}{2}\frac{|y|}{r^2}\left(\frac{1}{r_2}-\frac{r_2}{r}\right) ,$$

$$v_{2,2,E}(x,y) = f_\infty\frac{d^2}{2}\frac{\mathrm{sign}(y)}{r}\cdot \left(-\frac{1}{r_2}-\frac{x}{r_2 r}+\frac{x}{r^2}\frac{r_2}{}\right) , \quad (24)$$

with $r = \sqrt{x^2+y^2}$, $r_2 = \sqrt{2r+2x}$, $\lambda = 1$, and with

$$f(z) = -\frac{1}{\sqrt{2\pi}}\,\mathrm{erf}(\frac{z}{\sqrt{2}}) + \frac{1}{2\sqrt{\pi}}\,\mathrm{erf}(\frac{z}{2})\,e^{-\frac{z^2}{4}} , \quad (25)$$

where

$$\mathrm{erf}(z) = \frac{2}{\sqrt{\pi}}\int_0^z \exp(-\zeta^2)\,d\zeta .$$

Finally,

$$f_\infty = \lim_{z\to\infty} f(z) = -\frac{1}{\sqrt{2\pi}} . \quad (26)$$

5. Numerical implementation and results

The equations (1) have been implemented in Comsol for Reynolds numbers between one and 4000. For computational purposes we have chosen units such that the length of the segment A, the viscosity μ, and the speed at infinity u_∞ equal one. With such units the Reynolds number Re is equal to the density ρ of the fluid, which has been varied between one and 4000. Two types of boundary conditions have been used, namely constant boundary conditions, corresponding to setting $N = 0$ in (17) and adaptive boundary conditions of order $N = 2$. The computations have been performed in two computational domains $\mathbf{D}$, a square of side length 40 centered at the origin and a disk of radius 5 centered at the origin. For the case of the square the errors between the drag computed for the two boundary conditions is small, and the results fit very well the theoretical prediction (8) obtained from asymptotic expansions. See Figure 3.

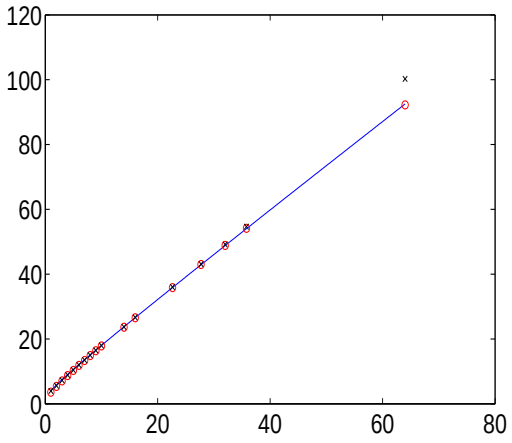

Fig 3. Drag on the segment as a function of $\mathrm{Re}^{1/2}$, computed in a square of size 40 The blue curve is the theoretical prediction based on (8). The black crosses are the values of the drag computed with constant boundary conditions. The red circles are the values of the drag computed with second order adaptive boundary conditions.

For a disk of radius five the constant boundary conditions give poor results, but the second order adaptive conditions continue to be very accurate. See [3] and [4] for a systematic study of the adaptive boundary

conditions.

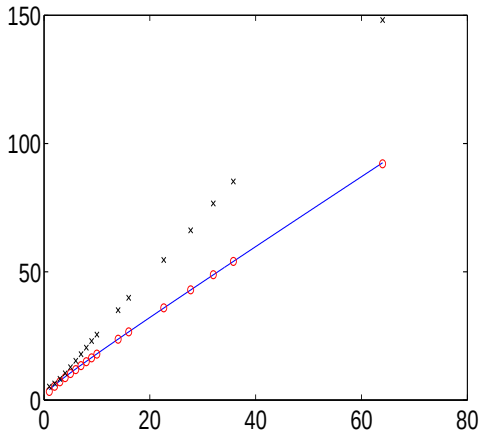

Fig 4. Drag on the segment as a function of $\mathrm{Re}^{1/2}$, computed in a disk of radius 5. The blue curve is the theoretical prediction based on (8). The black crosses are the values of the drag computed with constant boundary conditions. The red circles are the values of the drag computed with second order adaptive boundary conditions.

We now illustrate the physics behind this dramatic improvement in the quality of the results when choosing adequate boundary conditions. Figure 4 shows the streamlines of the vector field $\mathbf{u} - \mathbf{u}_\infty$, where $\mathbf{u}$ solves the Navier-Stokes equations (1) and where $\mathbf{u}_\infty = (u_\infty, 0)$. For the constant boundary conditions this vector field is equal to zero on the boundary S, which leads to a nonphysical low speed back-flow of the fluid extending over most of the computational domain.

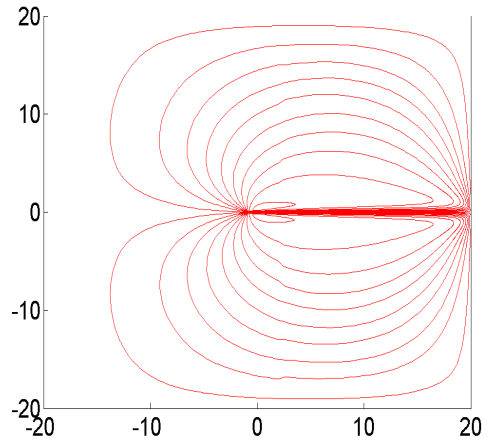

Fig 4. Non-physical back-flow induced by constant boundary conditions.

Figure 5 shows again the streamlines of the vector field $\mathbf{u}-\mathbf{u}_\infty$, but the solution has been computed using the second order adaptive boundary conditions. The non-physical back-flow has completely disappeared, and no distortion of the stream-lines is visible at the outer boundary.

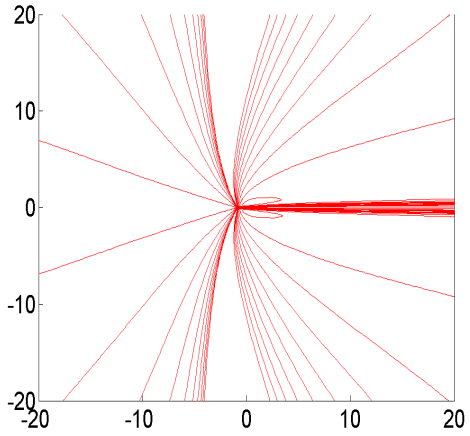

Fig 5. For adaptive boundary conditions no non-physical back-flow is induced.

6. Conclusions

We have shown that the computation of drag (and lift) is delicate for low Reynolds number flows since they depend sensitively on the boundary conditions. This problem can be avoided by using the proposed simple to implement adaptive boundary conditions. We have shown furthermore, that for the computation of lift and drag the integration over rough boundaries can be avoided by integrating over the outer boundary of the computational domain.

7. References

[1] M. Abdulrahim and J. Cocquyt. Development of mission-capable flexible-wing micro air vehicles. Technical report, University of Florida, 2000.

[2] Denis Bichsel and Peter Wittwer. Stationary flow past a semi-infinite flat plate: analytical and numerical evidence for a symmetry-breaking solution. *Journal of Statistical Physics*, online first, 2007.

[3] Sebastian Bönisch, Vincent Heuveline, and Peter Wittwer. Adabtive boundary conditions for exterior flow problems. *Journal of Mathematical Fluid Mechanics*, 7:85–107, 2005.

[4] Sebastian Bönisch, Vincent Heuveline, and Peter Wittwer. Second order adaptive boundary conditions for exterior flow problems: non-symmetric stationary flows in two dimensions. *Journal of mathematical fluid fechanics*, 8:1–26, 2006.

[5] R. Eppler and D. M. Somers. Low speed airfoil design and analysis. *Advanced Technology Airfoil Research, Volume I*, 1:73–100, 1979.

[6] R. Eppler and D. M. Somers. *A Computer Program for the Design and Analysis of Low-Speed Airfoils*, 1981.

[7] R. Eppler and D. M. Somers. Airfoil design for Reynolds numbers between 50, 000 and 500, 000. In *Conference on Low Reynolds Number Airfoil Aerodynamics*, pages 1–14, 1985.

[8] E. S. Hanf. Piv application in advanced low Reynolds number facility. *IEE Transactions on Aerospace and Electronic Systems*, 40:310–319, 2004.

[9] V. Heuveline and P. Wittwer. Exterior flows at low reynolds numbers: concepts, solutions and applications. 2007.

[10] C. L. Ladson, C. W. Brooks, Jr., A. S. Hill, and D. W. Sproles. Computer program to obtain ordinates for NACA airfoils. Technical report, NASA, 1996.

[11] P. B. S. Lissaman. Low-Reynolds-number airfoils. preprint, 1983.

[12] R. I. McLachlan. The boundary layer on a finite flat plate. *Phys. Fluids A*, 3:341–348, 1991.

[13] T. J. Mueller. *Fixed and Flapping Wing Aerodynamics for Micro Air Vehicle Applications*, volume 195. AIAA, 2001.

[14] Thomas J. Mueller and James D. DeLaurier. Aerodynamics of small vehicles. *Annual review of Fluid Mechanics*, 35:89–111, 2003.

[15] A. Pelletier and T.J. Mueller. Low Reynolds number aerodynamics of low-aspect-ratio, thin/flat/cambered-plate wings. *Journal of Aircraft*, 37(5):825–832, 2000.

[16] H. Schlichting and K. Gersten. *Boundary layer theory*. Springer, 1999.

[17] H. Werle. *Le tunnel hydrodynamique au service de la recherche aérospatiale, Publication No 156*. ONERA, Oficce National d'études et de recherches aérospaciales, 1974.

[18] P. Wittwer. On the structure of Stationary Solutions of the Navier-Stokes equations. *Commun. Math. Phys.*, 226:455–474, 2002.